



# Impacts of atmosphere–sea ice–ocean interaction on Southern Ocean deep convection in a climate system model

Libin Ma<sup>1,2</sup> · Bin Wang<sup>3</sup> · Jian Cao<sup>2</sup>

Received: 23 May 2019 / Accepted: 16 March 2020 / Published online: 24 March 2020  
© Springer-Verlag GmbH Germany, part of Springer Nature 2020

## Abstract

Deep convection in polar oceans plays a critical role in the variability of global climate. In this study, we investigate potential impacts of atmosphere–sea ice–ocean interaction on deep convection in the Southern Ocean (SO) of a climate system model (CSM) by changing sea ice–ocean stress. Sea ice–ocean stress plays a vital role in the horizontal momentum exchange between sea ice and the ocean, and can be parameterized as a function of the turning angle between sea ice and ocean velocity. Observations have shown that the turning angle is closely linked to the sea-ice intrinsic properties, including speed and roughness, and it varies spatially. However, a fixed turning angle, i.e., zero turning angle, is prescribed in most of the state-of-the-art CSMs. Thus, sensitivities of SO deep convection to zero and non-zero turning angles are discussed in this study. We show that the use of a non-zero turning angle weakens open–ocean deep convection and intensifies continental shelf slope convection. Our analyses reveal that a non-zero turning angle first induces offshore movement of sea ice transporting to the open SO, which leads to sea ice decrease in the SO coastal region and increase in the open SO. In the SO coastal region, the enhanced sea-ice divergence intensifies the formation of denser surface water descending along continental shelf by enhanced salt flux and reduced freshwater flux, combined with enhanced Ekman pumping and weakened stratification, contributing to the occurrence and intensification of continental shelf slope convection. On the other hand, the increased sea ice in the open SO weakens the westerlies, enhances sea-level pressure, and increases freshwater flux, whilst oceanic cyclonic circulation slows down, sea surface temperature and sea surface salinity decrease in the open SO response to the atmospheric changes. Thus, weakened cyclonic circulation, along with enhanced freshwater flux, reduced deep–ocean heat content, and increased stability of sea water, dampens the open–ocean deep convection in the SO, which in turn cools the sea surface temperature, increases sea-level pressure, and finally increases sea-ice concentration, providing a positive feedback. In the CSM, the use of a non-zero turning angle has the capability to reduce the SO warm bias. These results highlight the importance of an accurate representation of sea ice–ocean coupling processes in a CSM.

**Keywords** The southern ocean · Sea ice–ocean stress · Turning angle · Open–ocean deep convection · Sea-ice divergence · Freshwater flux · Atmosphere–sea ice–ocean interaction

## 1 Introduction

Deep convection is an important ocean process, which transports warm water from deep ocean to surface. Two types of deep convection usually occur in the polar region during winter (e.g., Killworth 1983). The first type appears at the continental shelf where the cold water sinks along the slope (referred to as “continental shelf slope convection”). Because of the brine rejection caused by the formation of sea ice and the offshore katabatic wind, the dense salty water formed on the shelf descends along the slope and entrains the warm deep water upward. The other type of convection is called open–ocean deep convection. It is observed in

**Electronic supplementary material** The online version of this article (<https://doi.org/10.1007/s00382-020-05218-1>) contains supplementary material, which is available to authorized users.

- ✉ Libin Ma  
malibin109@163.com
- ✉ Bin Wang  
wangbin@hawaii.edu

Extended author information available on the last page of the article

the Labrador and Greenland seas, Mediterranean Sea, and Weddell Sea (Killworth 1983; Marshall and Schott 1999). Open-ocean deep convection commonly occurs in regions of a cyclonic current system with a preconditional surface cooling in the early winter.

Previous studies showed that open-ocean deep convection causes significant changes in the properties of sea water. Through associated physical processes including the thermobaric effect, open-ocean deep convection causes changes in seawater temperature and salinity, and hence the density (Akitomo 1999a, b). Furthermore, the water exchange between cold surface water and warm deep water in the convective region enhances the heat loss to the atmosphere, which may strengthen the Atlantic Meridional Overturning Circulation (AMOC; Delworth et al. 1993; Dong and Sutton 2001; Danabasoglu 2008; Frankignoul et al. 2009; Msadek and Frankignoul 2009; Jackson and Vellinga 2012; Roberts et al. 2013).

Different from the frequent occurrence of open-ocean deep convection in the northern North Atlantic, there is a rare but natural occurrence of the open-ocean deep convection in the Southern Ocean (SO). Only one large open-ocean deep convection event was observed in the Weddell Sea, which happened in 1974–1976 (Gordon and Comiso 1987). Gordon (1978, 1982) found that the warm deep water in the Weddell Sea in the convective years was much colder than that in 1973. The process influenced the formation of other water masses in the Weddell Sea, such as deep and bottom waters (Fahrbach et al. 1995), and thus the Antarctic Bottom Water (AABW) (Orsi et al. 1999). On the other hand, the results from the Coupled Model Intercomparison Project phase 5 (CMIP5) showed that some models have open-ocean deep convection but others lack such convection under pre-industrial conditions (de Lavergne et al. 2014). The open-ocean deep convection in the CMIP5 models has diverse frequency variation, as its timescale ranges from decadal, multidecadal to centennial (Martin et al. 2013). Once the open-ocean deep convection occurs, the local water properties are significantly modified. With the results of CMIP5 models, Heuzé et al. (2013) assessed the formation processes of dense water, and concluded that the models with deep convection in the Weddell and Ross seas have realistic bottom-water properties. With CMIP5 models and a coupled atmosphere–ocean–chemistry–climate model (Morgenstern et al. 2014), Behrens et al. (2016) found that strong deep convective activities reduce sea-ice cover, weaken sub-polar gyres, and enhance Drake Passage transport.

What is responsible for the formation of open-ocean deep convection in the SO? Owing to the weak stratification (Gordon and Huber 1990), open-ocean deep convection has been thought to be induced by (1) brine rejection, i.e., the sea-ice freezing (Martinson 1991), (2) the interaction between currents and the Maud Rise Seamount (Holland 2001),

and (3) precipitation–evaporation flux (Gordon et al. 2007; Galbraith et al. 2011). Using a global ocean–sea ice model, Hirabara et al. (2012) showed that the anomalously warm deep water, saline surface layer, and cyclonic wind stress over the deep convective region in early winter can trigger a winter–persisting open-ocean deep convection. They also pointed out that the formation of open-ocean deep convection in the Weddell Sea is related to surface air temperature. Other coupled sea ice–ocean model results showed that the cyclonic Weddell gyre is intensified with the strengthening of westerlies, which further raises the warm deep water to the surface (Cheon et al. 2014, 2015, 2018) because of the doming of isopycnals (Robertson et al. 2002). Hence, the formation of open-ocean deep convection is closely linked to the open-ocean polynyas, suggesting the important role of sea-ice dynamics in the SO (e.g., Gordon 1982; Wang et al. 2017; Cheon et al. 2018).

Based on previous studies, the mechanisms related to the formation of open-ocean deep convection can be grouped into two types (e.g., Smith et al. 1990; Morales Maqueda et al. 2004): mechanical forcing and convective forcing (Williams et al. 2007). The mechanical forcing is associated with sea-ice divergence, whereas oceanic heat flux is the main cause of the convective forcing. In addition, the wind-driven sea-ice motion plays a vital role in ocean ventilation in the SO (e.g., Saenko et al. 2002). The sea-ice divergence induced by wind forcing, i.e., offshore katabatic winds, excites northward sea-ice freshwater transport to the open ocean, modulating the local coupled climate system (Born et al. 2010; Haumann et al. 2016).

In this work, we hypothesize that the sea ice–ocean stress influences the properties of open-ocean deep convection. Sea ice acts as a medium isolating the upper ocean from the cold air in polar regions and exerts a profound impact on the atmosphere–ocean interaction. There is a stress at the sea ice–ocean interface, which represents the momentum exchange in a thin ocean layer (Fig. 1a). Thus, the total stress exerted on the ocean in a coupled climate model can be formulated as follows,

$$\tau = (1 - F_{ice})\tau_{AO} + F_{ice}\tau_{IO}, \quad (1)$$

where  $\tau_{AO}$  is the stress imposed by the wind on the ice-free ocean,  $\tau_{IO}$  is the kinematic sea ice–ocean stress, and  $F_{ice}$  is sea-ice concentration. It has been known that variation of  $\tau_{AO}$  can significantly influence the deep convection in the SO via open-ocean polynyas (Cheon et al. 2014, 2015, 2018; Wang et al. 2017). However, the total stress imparted on the ice-covered ocean is modulated by the variations of  $\tau_{AO}$  and  $\tau_{IO}$  in the climate system model (CSM).

Will changes in sea ice–ocean stress influence the properties of open-ocean deep convection in the SO? If it does, how does the sea ice–ocean stress affect the SO open-ocean

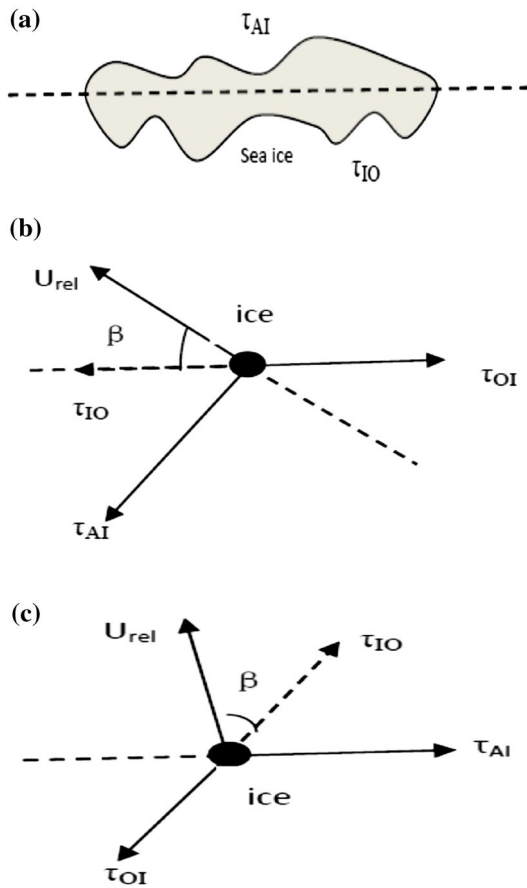


**Fig. 1** **a** Interface between sea ice and ocean. Schematic diagrams showing force balance of an ice pack in **(b)** the Northern Hemisphere and **(c)** Southern Hemisphere, respectively.  $U_{rel} = \mathbf{u}_i - \mathbf{u}_o$  is the relative velocity of sea ice with respect to ocean.  $\tau_{AI}$ ,  $\tau_{OI}$ , and  $\tau_{IO}$  are the air-sea ice, ocean-sea ice, and sea ice-ocean stresses, respectively

deep convection? These questions are addressed in this study. Particular attention is paid to the parameterization of the sea ice–ocean stress. In ocean models, the kinematic sea ice–ocean stress is parameterized in the following form (e.g., Zika et al. 2013):

$$\tau_{IO} = \rho_w c_w (\mathbf{u}_i - \mathbf{u}_o) |\mathbf{u}_i - \mathbf{u}_o| e^{\pm i\beta}, \quad (2)$$

where  $\rho_w$  is seawater density,  $c_w$  is the drag coefficient,  $\mathbf{u}_i - \mathbf{u}_o$  is the relative velocity between sea-ice velocity  $\mathbf{u}_i$  and seawater velocity  $\mathbf{u}_o$ , and  $\beta$  the turning angle between the relative velocity  $\mathbf{u}_i - \mathbf{u}_o$  and the sea ice–ocean stress  $\tau_{IO}$ , ranging from  $0^\circ$  to  $23^\circ$  (Hunkin 2010; Uotila et al. 2012). Observations have shown that ocean currents deflect to the right of sea-ice drift in the Arctic Ocean (Hunkins 1966) (Fig. 1b), whereas they deflect to the left in the Antarctic Ocean (Defant 1961) (Fig. 1c) due to the Ekman drift. In addition, uncertainties exist in the parameterization of sea ice–ocean stress. It should be noted that  $c_w$  and  $\beta$  are,

respectively, taken as constant values in most coupled atmosphere–sea ice–ocean models, say, setting  $c_w$  and  $\beta$  to 0.0055 and  $0^\circ$ , respectively (e.g., Hunke and Lipscomb 2010; Hurrell et al., 2013). However, McPhee (1980) suggested setting  $\beta$  to  $23^\circ$  relative to the geostrophic ocean current. Given the hydraulic roughness, moreover, McPhee (2012) argued that both  $c_w$  and  $\beta$  are functions of sea-ice speed. On the other hand, it is claimed that a turning angle is not necessary if the Ekman spiral, which is activated in the Ekman layer and decays by an e-folding over a depth as the current vector rotates to the left (right) in the Southern (Northern) hemisphere, can be resolved in the top ocean model layers (Hunkin 2010). Additionally, the Ekman depth is related to the vertical turbulent viscosity  $v_E$  and Coriolis parameter  $f$ , and is estimated by  $\sqrt{2v_E/|f|}$ . Note that  $v_E$  usually takes the value of  $10^{-4}$ – $10^{-2}$  m $^2$  s $^{-1}$  in most ocean general circulation models (OGCMs) and CSMs. Thus, the Ekman depth has the value of O(1)–O(10) m south of  $60^\circ$ S. Moreover, Chu (2015) theoretically addressed that the e-folding depth of the Ekman layer is no deeper than 5 m in the high latitudes (see his Fig. 15 for detail). However, the first layer of most CSMs is placed at the depth of O(10) m (Park et al. 2009; Ge et al. 2017; Cao et al. 2018), which cannot well resolve the Ekman spiral. Thus, it is necessary to take a non-zero turning angle into consideration for the CSMs that have coarse vertical resolution in the ocean component, especially in the top ocean, including the coupled model used in this study.

We will discuss whether and how the variation of  $\beta$  exerts the influence on the SO open–ocean deep convection in this study, by using a coupled atmosphere–ocean–land–sea ice model. A brief description of the coupled model and the corresponding experimental design are described in Sect. 2. In Sect. 3, the observed climatologies of sea surface temperature (SST), sea surface salinity (SSS), and surface ocean currents averaged in the austral winter (June–July–August, or JJA) are briefly discussed. Sensitivity of SO deep convection to the turning angle  $\beta$  is illustrated in Sect. 4; associated changes in the ocean, sea ice, and atmosphere response to the atmosphere–sea ice–ocean interaction are discussed in Sect. 5. We then show the corresponding mechanism and physical processes controlling the response of SO deep convection to the turning angle in Sect. 6. Summary and discussion are presented in Sect. 7.

## 2 Model description, experimental design, and method

### 2.1 Models

The model employed here is the third generation of the Nanjing University of Information Science and Technology Earth System Model (NESM3.0) (Cao et al.

2018). NESM3.0 consists of the atmospheric component ECHAM6.3.02 (Stevens et al. 2013), which includes the land model JSBACH (Raddatz et al. 2007), the ocean component NEMO3.4 (Madec 2012), and the sea-ice component CICE4.1 (Hunke and Lipscomb 2010). Component models are coupled by the Ocean–Atmosphere–Sea-Ice–Soil Model Coupling Toolkit (OASIS-MCT3.0) (Valcke and Coquart 2015). The low-resolution (LR) version of NESM3.0 is used in this study. The horizontal resolution of the atmosphere and land models is T31, which is about  $3.75^\circ$  in both directions; and the atmosphere model has 31 levels in the vertical direction, extending from the surface to 1.0 hPa. The ocean component is ORCA2, which has a resolution of approximately  $2^\circ \times 2^\circ$  with refinement in the tropical region; it has 31 layers in the vertical direction with the first layer placed at 5 m and 10 layers in the upper 100 m with 10-m interval, which does not well resolve the Ekman spiral in the top ocean. The sea-ice component has a resolution of about  $1/2^\circ \times 1^\circ$  in the meridional and zonal directions.

## 2.2 Experimental design

To investigate the influence of the turning angle  $\beta$  on SO deep convection, two values of  $0^\circ$  and  $20^\circ$  are selected. Experiments with these two values are named ANG00 and ANG20, respectively; the former is referred to as the control. Note that other non-zero turning angles, i.e.,  $5^\circ$ ,  $10^\circ$ , and  $15^\circ$ , are also tested, and they showed similar qualitative results as those of  $\beta = 20^\circ$  (Fig. S1). Starting from the same initial conditions, both runs are integrated for 1000 years under the pre-industrial conditions, and the last 300 years are used for analysis. Monthly mean outputs are used for both ocean and sea ice. The time interval of atmosphere output is set to 6 h. Thus, the monthly mean outputs of atmosphere are calculated based on the 6-h data.

To further explore how the non-zero turning angle influences the atmosphere–sea ice–ocean interaction, three sensitivity experiments are added, which can answer the following questions: (1) how does the sea-ice distribution respond to change in turning angle? (2) how does the atmosphere react to the change in sea-ice pattern? and (3) how does the ocean respond to atmospheric changes? To address question (1), sensitivity experiment ANG20\_WND00 is conducted, which has the same settings as ANG20 except that the surface wind stresses from ANG00 are used to drive the ocean and sea ice at each time step of the integration. Note that we only substitute the surface wind stresses in the ocean and sea-ice components in ANG20\_WND00. The changed surface wind stresses do not directly interfere with any process in the atmosphere, whereas the feedbacks resulting from changes in ocean and sea-ice states can interact with associated atmospheric processes. To address question (2), sensitivity experiment ANG00\_ICE20 is implemented based

on ANG00, but the sea-ice state, including sea-ice concentration and albedo, is obtained from ANG20 used as the boundary conditions of atmosphere during the integration. To address question (3), a mirrored sensitivity experiment ANG00\_WND20 is implemented based on ANG00, but the surface wind stresses obtained from ANG20 is used for the ocean and sea-ice models. ANG20\_WND00, ANG00\_ICE20, and ANG00\_WND20 start from the model year 700 of ANG20, ANG00, and ANG00, respectively, and are integrated for 300 years each.

## 2.3 Methods

Some basic measures based on mixed layer depth (MLD) are defined here to evaluate the deep convection, including open-ocean deep convection and continental shelf slope convection. CMIP5 recommends using the density criterion of  $0.125 \text{ kg m}^{-3}$  to estimate the MLD, which is the difference of potential density relative to the surface density. However, the SO is weakly stratified, so CMIP5's method will yield large MLD in winter. Hence, the MLD in this study is defined by using a density criterion of  $0.01 \text{ kg/m}^3$  (e.g., Reintges et al. 2017). Following previous studies, we define September MLD as the maximum MLD (e.g., de Lavergne et al. 2014). Note that other criteria, such as  $0.03 \text{ kg/m}^3$  used in de Lavergne et al. (2014), to calculate the MLD have been tested in our study, and these results showed no significant difference. Following de Lavergne et al. (2014), an open-ocean convective event occurs when the September MLD exceeds 2000 m. A convection year is identified when the convection area exceeds the threshold of  $250,000 \text{ km}^2$ , which is the observed value in the 1970s for the polynya area in the Weddell Sea (Gordon and Comiso 1987). Furthermore, similar to the definition of Reintges et al. (2017), the main convection region of each experiment coincides with the area where the September MLD exceeds 2000 m and accounts for at least 5% of the 300-year data. Note that there is a high correlation between the convection area and mixed layer volume (MLV), which is calculated by integrating the water column with the MLD exceeding 2000 m horizontally in the convection area (e.g., Behrens et al. 2016; Reintges et al. 2017). The convection area is used to measure the strength of open-ocean deep convection in this study.

The sea-ice freshwater transport,  $\mathbf{f}$  ( $\text{m}^2 \text{ s}^{-1}$ ), is calculated following Haumann et al. (2016):

$$\mathbf{f} = C_{fw} c h \mathbf{u}_i, \quad (3)$$

where  $c$ ,  $h$ , and  $\mathbf{u}_i$  are sea-ice concentration, thickness, and drift velocity, respectively.  $C_{fw}$  is the factor measuring the conversion of sea-ice volume flux to the freshwater equivalent (Ohshima et al. 2014) and has the following form:

$$C_{fw} = \frac{\rho_{ice} \left(1 - S_{ice}/S_{sw}\right)}{\rho_{fw}}, \quad (4)$$

where  $S_{ice}$ ,  $S_{sw}$ ,  $\rho_{ice}$ , and  $\rho_{fw}$ , respectively, are sea-ice salinity ( $6 \text{ g kg}^{-1}$ ), the reference seawater salinity ( $34.7 \text{ g kg}^{-1}$ ), sea-ice density ( $925 \text{ kg m}^{-3}$ ), and freshwater density ( $1000 \text{ kg m}^{-3}$ ).

## 2.4 Validation of the model stability

Figure 2 shows the time series of global mean SST, SSS, and the energy budget at the top of atmosphere (TOA). The global mean SSTs averaged over the 300-year period in ANG00 and ANG20 are  $17.63^\circ\text{C}$  and  $17.48^\circ\text{C}$ , respectively

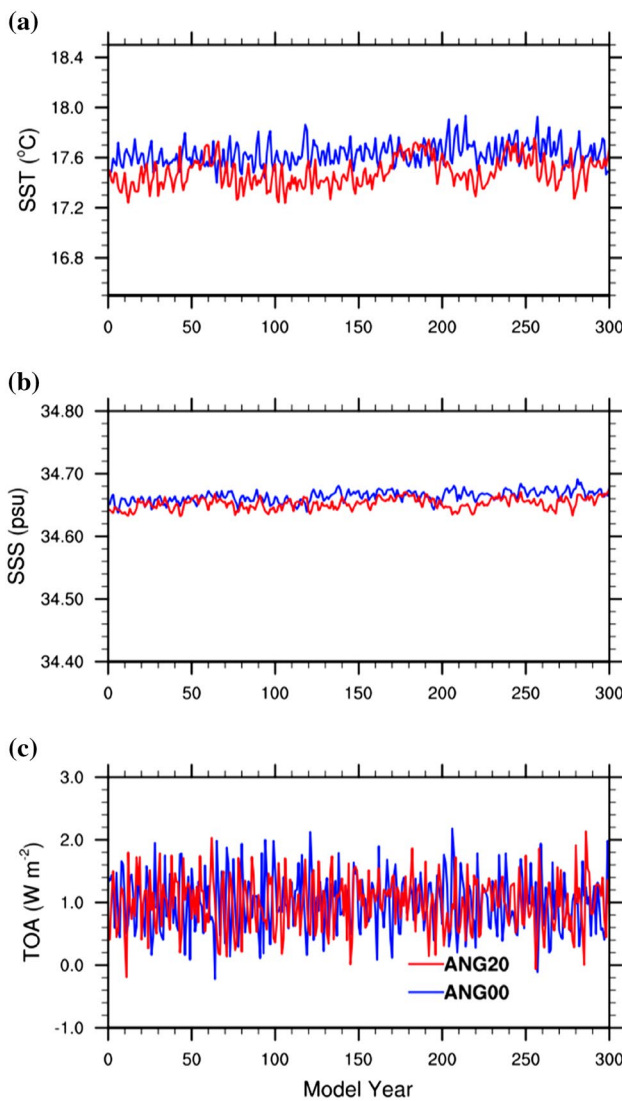


**Fig. 2** Time series of global mean **a** sea surface temperature ( $^\circ\text{C}$ ), **b** sea surface salinity (psu), and **c** top-of-atmosphere energy budget ( $\text{W/m}^2$ )

(Fig. 2a). The trends of global-mean SST in ANG00 and ANG20 are  $0.03$  and  $0.04^\circ\text{C}$  per century ( $^\circ\text{C}/100$  year), respectively. In ANG00 and ANG20, the global mean SSS values are  $34.66$  and  $34.65$  psu, respectively; and the trends of global mean SSS are  $0.01$  and  $0.04$  psu/ $100$  year, respectively. Moreover, the TOA energy budgets in ANG00 and ANG20 are  $0.996$  and  $0.992 \text{ W/m}^2$ , respectively; and the corresponding trends are  $-0.018$  and  $-0.02 \text{ W/m}^2/100$  year, respectively. The insignificant trends in SST, SSS, and TOA energy budget demonstrate that both ANG00 and ANG20 have reached steady states, and their results are adequate for our analyses.

## 3 Observed climatology of SST, SSS, and surface currents

Figure 3 shows the JJA-mean SST, SSS, and surface currents, which are derived from the ORAS4 (Balmaseda et al. 2013). ORAS4 is a reanalysis product, and taken as “observations” in this study. The ORAS4 data used in this study cover the period from 1958 to 2010, and the horizontal resolution is  $1^\circ \times 1^\circ$ . As illustrated by the dashed line ( $-1.8^\circ\text{C}$ , referred to as the threshold of the freezing of sea ice, the Antarctic Ocean is generally covered by sea ice in winter (Fig. 3a). Apart from cold water, fresh surface water is also found at high latitudes of the SO, except in the Weddell Sea (Fig. 3b). In the Weddell Sea, the water is more saline than the surrounding water, probably caused by the brine rejection during sea-ice freezing. Regarding the currents, a cyclonic circulation, which is one of the preconditions for the formation of open-ocean deep convection, is found in the Weddell Sea (Fig. 3c). It should be pointed out that the ORAS4 missed the observed open-ocean deep convection that occurred in the winter season from 1974 to 1976 (figure not shown). Despite of that, the above-mentioned properties of ORAS4 data can be used as reference for explaining why our model results show different behaviors of open-ocean deep convection in the SO.

## 4 Southern Ocean deep convection response to changes in sea ice–ocean stress

MLD is usually taken as a proxy to represent the activity of deep convection (e.g., de Lavergne et al. 2014; Reintges et al. 2017). Figure 4 depicts the standard deviation of MLD and frequency of deep-convective events in September, which reflect the variability and strength of deep convection. Note that the frequency of deep-convective events is calculated as the ratio of number of convective years to the total model years. Regions with a larger standard deviation

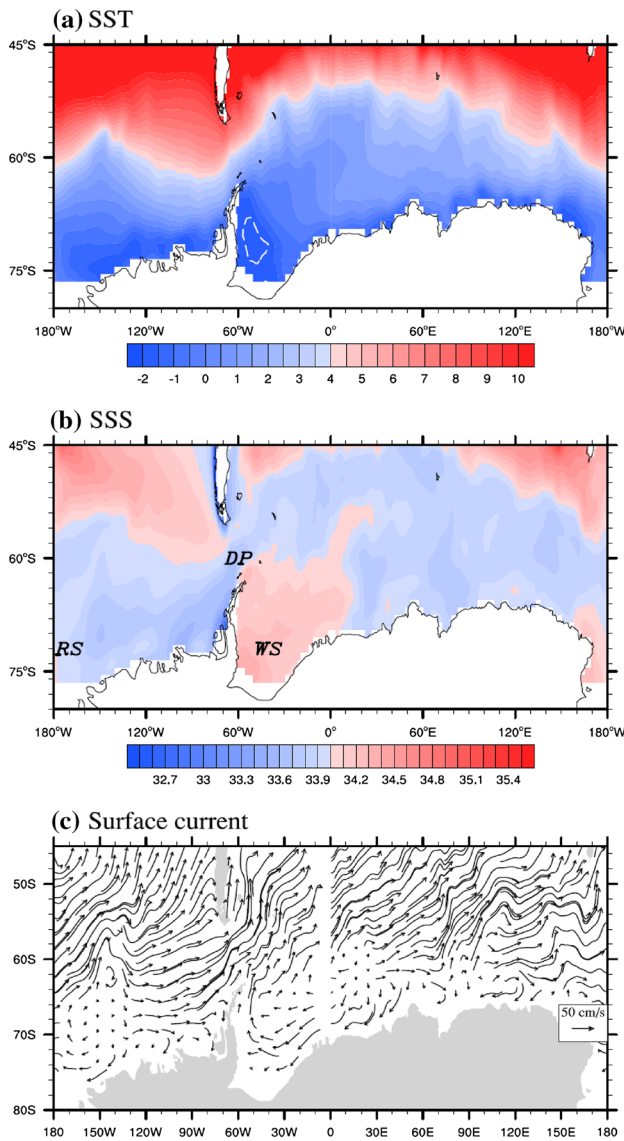


**Fig. 3** JJA-mean **a** sea surface temperature (SST; °C), **b** sea surface salinity (SSS; psu), and **c** surface ocean currents (cm/s) derived from ORAS4. The dashed white contour in (a) denotes the  $-1.8^{\circ}\text{C}$  isoline. “RS”, “DP”, and “WS” in (b) denote the Ross Sea, Drake Passage, and Weddell Sea, respectively

of MLD, in general, have a larger climatological MLD (figure not shown). As shown in Fig. 4a, if turning angle is zero, large MLD variability is found mainly in the open ocean of the South Atlantic from  $40^{\circ}\text{W}$  to  $40^{\circ}\text{E}$ . A relatively large variability of MLD is also found in the open ocean at the western part of the Indian sector of the SO (Fig. 4a). In the presence of the turning angle in ANG20, smaller MLD standard deviations are found in the open ocean (Fig. 4b), implying that the variability of open-ocean deep convection is weakened. Opposite to the open ocean, the coastal region in ANG20 shows enhanced variability of MLD, suggesting that continental shelf slope convection occurs

more intermittently in ANG20, induced by the changes in ocean currents and atmospheric forcing. On the other hand, no open-ocean deep convection and continental shelf slope convection occur in the Ross Sea in the above-mentioned experiments, which is different from the results of some CMIP5 models, such as ACCESS1.0, ACCESS1.3, GFDL-CM3, GISS-E2-R, MIROC5, and MPI-ESM-MR (e.g., de Lavergne et al. 2014; Reintges et al. 2017).

To further explore the changes in deep convection, we estimate the frequency of deep-convective events at each model grid point. Compared to ANG00, ANG20 has a lower frequent occurrence of open-ocean deep convection but a higher frequent occurrence of continental shelf slope convection (Fig. 4c, d). Furthermore, the main convection region for each  $\beta$  is plotted (marked by the thin black isolines in Fig. 4c, d). The main convection region is defined as the area where the frequency of deep-convective events is higher than 0.05. Evidently, ANG00 has a larger main convection region in the Atlantic sector of the SO. In contrast, ANG20 has a larger convective area but weaker and less frequent open-ocean deep convection in the western part of the Indian sector of the SO. In this study, we only focus on deep convection that occurs in the South Atlantic sector (SAS; denoted by the black box in Fig. 4c, d) so as to make the analysis and discussion more concise. It should be pointed out that there are no significant changes in MLD between ANG00 and ANG20 in the North Atlantic.

## 5 Resultant atmosphere–sea ice–ocean interaction due to changes in sea ice–ocean stress

Changes in deep convection suggest that ocean state, as well as sea-ice state, has altered, whilst atmospheric state also changes because of the feedback effects of ocean and sea ice. Thus, the resultant atmosphere–sea ice–ocean interaction response to change in turning angle is discussed in this section.

### 5.1 Ocean response

Figure 5 depicts the JJA-mean SST and SSS, and the corresponding differences between ANG00 and ANG20. Note that the model results differ from those of the ORAS4, especially in the Atlantic and Indian sectors of the SO. Compared to the ORAS4, both ANG00 and ANG20 show warmer SST and higher SSS, especially in the eastern part of the Weddell Sea, suggesting that the deep-convection behaviors in the model are different from those of the ORAS4 (Figs. 3, 5). The dashed white contour ( $-1.8^{\circ}\text{C}$ ) in Fig. 5a, b suggests ANG00 and ANG20 have different spatial patterns of SST in the SO. The difference in SST, which is mainly found at

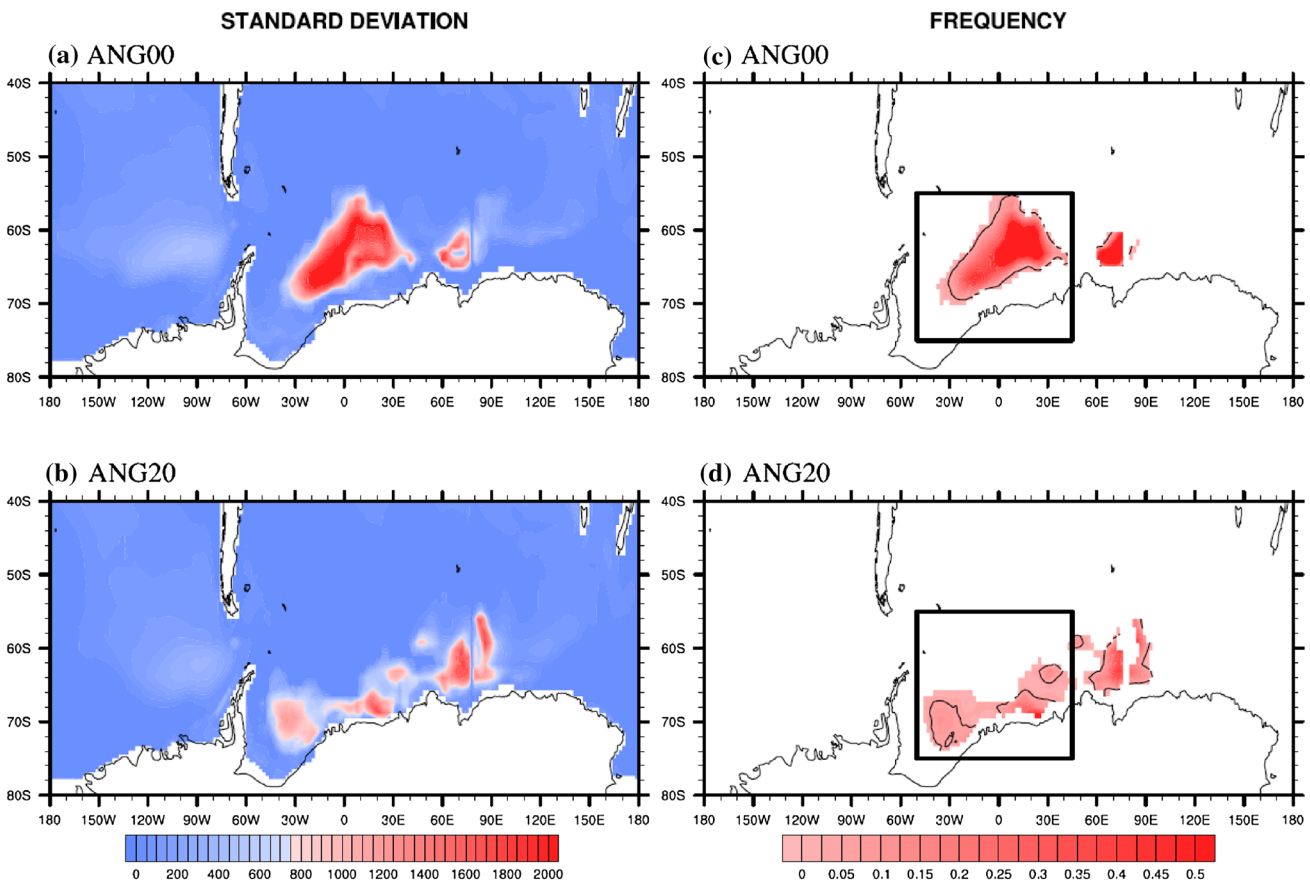


**Fig. 4** Standard deviation (left panels; m) and frequency (right panels) of September mean mixed layer depth (m) simulated from **(a, c)** ANG00 and **(b, d)** ANG20. The black box ( $50^{\circ}\text{W}$ – $45^{\circ}\text{E}$ ,  $55^{\circ}$ – $75^{\circ}\text{S}$ ) in **(c)** and **(d)** denotes the study area used in this study

the offshore side in the SO, centers around  $60^{\circ}\text{S}$  with colder water spanning from  $30^{\circ}\text{W}$  to  $150^{\circ}\text{W}$  and warmer water extending from  $150^{\circ}\text{W}$  to  $60^{\circ}\text{W}$  in ANG20 (Fig. 5c). A large area with decreased SST exists in the South Atlantic Ocean. Different from the SST in the open ocean, increased SST is seen along the Antarctic coast of the Atlantic and Indian sectors (Fig. 5c), including the southern and southeastern part of the Weddell Sea. Similar to the SST, the SSS is also different between ANG00 and ANG20 (Fig. 5d, e). Saltier water is found at both sides of the Drake Passage in ANG20, compared to ANG00 (Fig. 5f). On the other hand, fresher water is found in the regions of colder SST. Accompanying the positive SST difference, a positive SSS difference exists in the coastal region from  $60^{\circ}\text{W}$  to  $180^{\circ}$ . The dissimilarity in SST and SSS patterns between ANG00 and ANG20 may imply the disparate occurrence of open-ocean deep convection in the SO.

The distribution of mean surface ocean currents (at 5-m depth) in JJA is presented in Fig. 6. When turning angle is zero (Fig. 6a), a cyclonic gyre appears in the SAS, which is the precondition of the occurrence of open-ocean deep convection (Marshall and Schott 1999). The cyclonic ocean

currents in ANG20 are weaker (Fig. 6b), compared to those in ANG00. As a result, the westward Antarctic coastal currents in the South Atlantic and southern Indian Ocean sectors are weaker (Fig. 6c). Note that compared to ORAS4 (Fig. 3c), ANG00 and ANG20 show better organized cyclonic circulation in the SAS. This is consistent with the differences of SST and SSS in the SAS between the model results and ORAS4 data, that is, ANG00 and ANG20 simulate warmer and saltier surface water in the Weddell Sea.

## 5.2 Sea-ice response

How does the seasonal cycle of the sea-ice state respond to the change in turning angle? Fig. 7 shows the seasonal variations of sea-ice extent and volume in the Antarctic Ocean. Both model simulations capture the seasonal evolutions of sea-ice extent and sea-ice volume with the minimum and maximum sea-ice extent and volume occurring, respectively, in February–March (FM; the late austral summer and early fall) and September–October–November (SON; the austral spring). It is obvious that ANG20 has larger sea-ice extent than ANG00 during the entire year with the largest

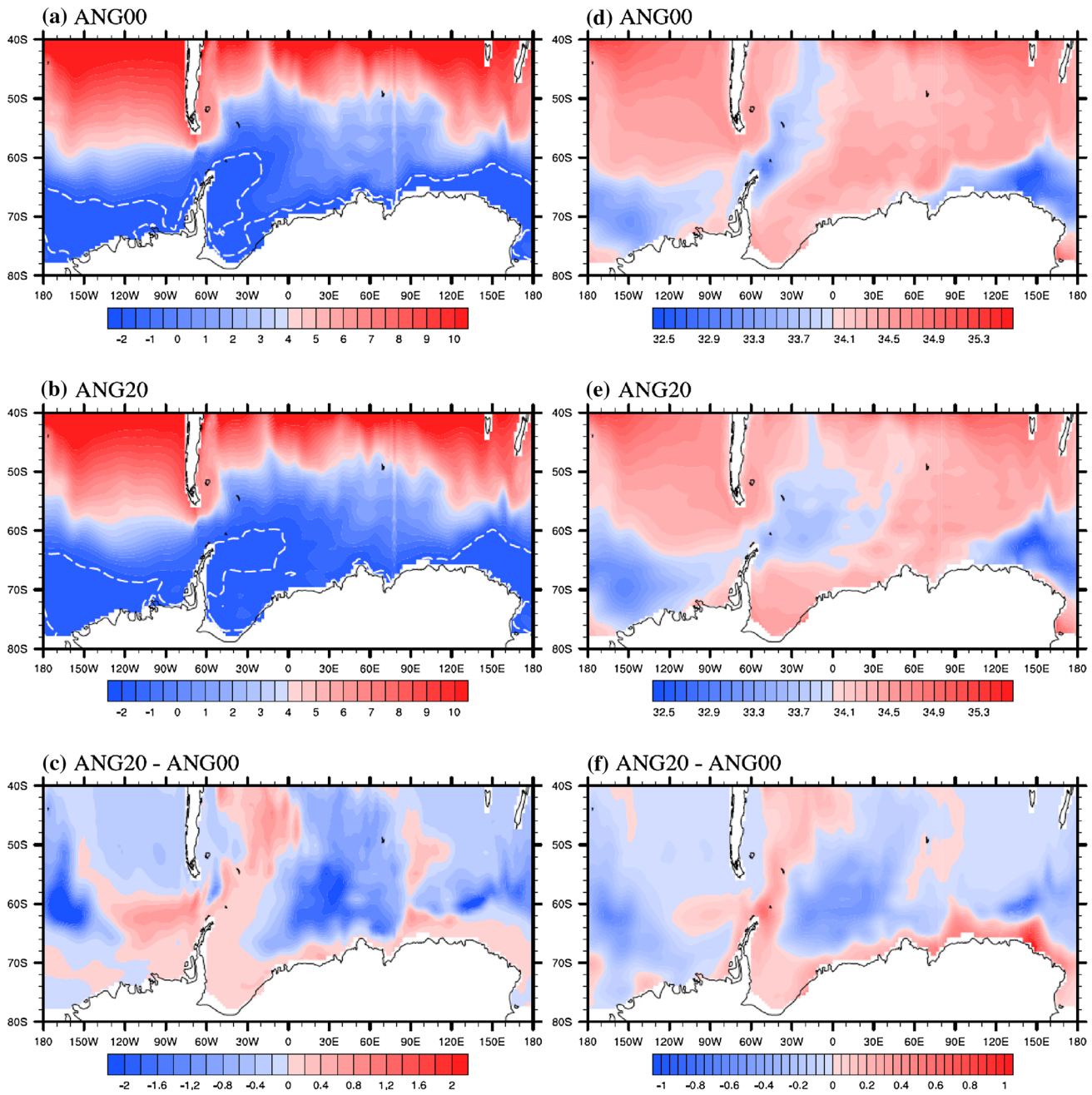


**Fig. 5** JJA-mean SST (left panels; °C) and SSS (right panels; psu) simulated in (a, d) ANG00, and (b, e) ANG20. **c, f** Denote the difference (ANG20 minus ANG00). The dashed white contours in (a) and (b) denote the  $-1.8\text{ }^{\circ}\text{C}$  isoline

discrepancy during SON (Fig. 7a). Regarding the sea-ice volume (Fig. 7b), ANG20 has less sea-ice volume in FM but larger sea-ice volume in SON. The enhanced sea-ice extent and volume in the austral winter are dominated by their increases in the SAS.

Figure 8 depicts the JJA mean during convective years and the corresponding differences in sea-ice drift, concentration, and thickness between ANG00 and ANG20. In comparison with ANG00, ANG20 has a larger domain covered

by sea ice in the SAS (shown by shading in Fig. 8a, b). Correspondingly, the sea-ice drift differs between ANG00 and ANG20 (shown by vectors in Fig. 8a, b). Along the coastal region, ANG20 has weaker sea-ice drift transporting less sea ice to the western Weddell Sea compared to ANG00 (Fig. 8c). Instead, ANG20 transports more sea ice northward to the open SAS, which contributes to the accumulation of sea ice over the open ocean (Fig. 8c). Similar to the distribution of sea-ice concentration (Fig. 8d–f), ANG20 has thinner

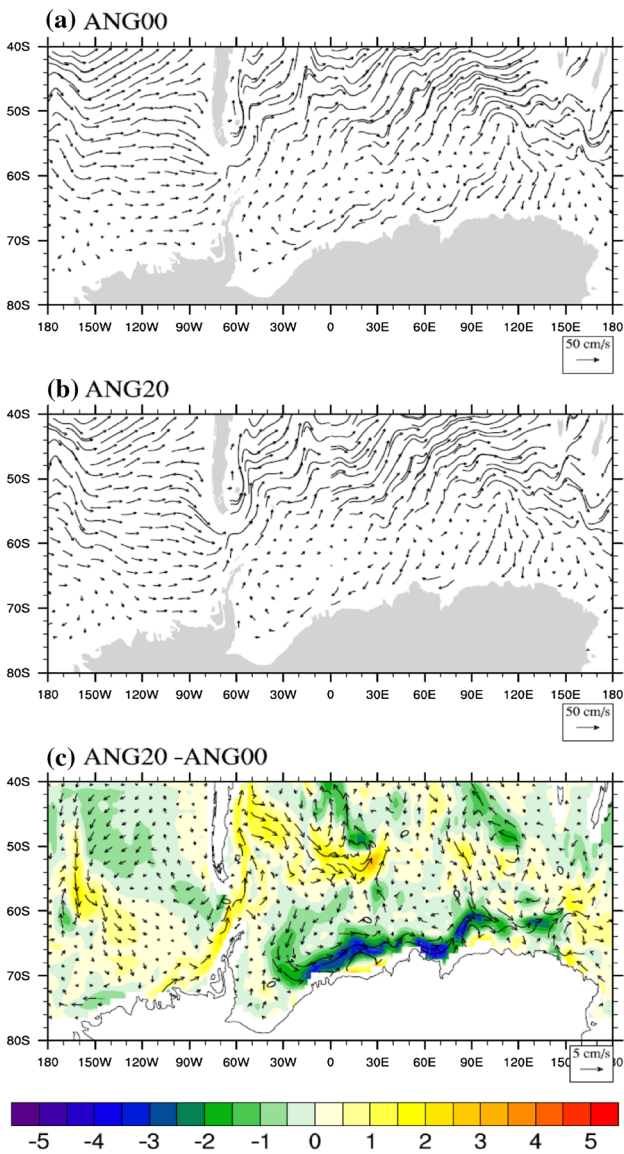


**Fig. 6** Same as Fig. 5, except for surface ocean currents (cm/s). The shading in (c) represents the difference of ocean current speeds between ANG20 and ANG00 ( $\text{ANG20} - \text{ANG00}$ )

sea ice in the western Weddell Sea and along the coastal region in the SAS. Note that the sea ice accumulates in the open ocean, which can survive through the next austral summer (the December–January–February season) (Fig. S2).

### 5.3 Atmospheric response

Changes in the ocean and sea ice states will cause variation of the atmosphere above. Because the ice packs accumulate in the open ocean and are not melted by the oceanic heat flux, there is a significant increase of sea-ice cover in the eastern SAS in ANG20 (Fig. 8c). The accumulated ice pack prevents sea water from being exposed to the atmosphere

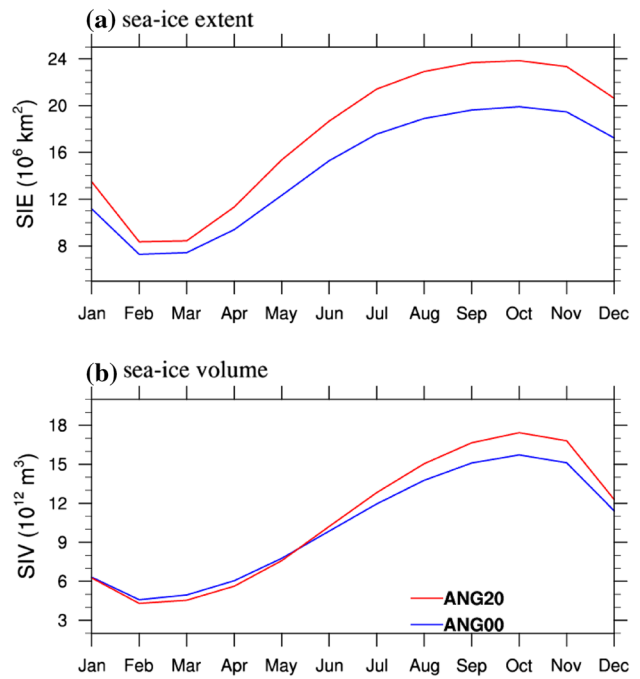


**Fig. 7** Seasonal variations of **a** sea-ice extent ( $10^6 \text{ km}^2$ ) and **b** sea-ice volume ( $10^{12} \text{ m}^3$ )

and alters the local atmosphere temperature, such as the 2-m air temperature is increased over the western SAS and coastal region and is decreased over the open ocean in the eastern SAS in ANG20 (figure not shown).

Previous studies showed that freshwater can exert a considerable influence on the occurrence of open-ocean deep convection (Gordon et al. 2007; Galbraith et al. 2011). As shown by Fig. 9a, b, ANG00 and ANG20 have different spatial distributions of P-E in the SAS during convective years. As discussed in Sect. 4.1, there is a large main convection area with stronger and more frequent open-ocean deep convection in ANG00 (Fig. 4a, c). Associated with these properties, a smaller amount of freshwater flux is released into the open ocean in ANG00 compared to ANG20, whilst ANG20 has less freshwater along the coastal region in the SAS (Fig. 9c). Less freshwater along the coastal region accompanied by stronger evaporation (figure not shown) tends to cause the surface water to be denser and to descend along the continental shelf, which contributes to the continental shelf slope convection (Martinson et al. 1981). On the other hand, more freshwater in the open SAS is assumed to play a vital role in weakening open-ocean deep convection in ANG20 (e.g., de Lavergne et al. 2014). The physical processes responsible for changes in the continental shelf slope convection and open-ocean deep convection are further discussed in the following section. In addition, the minimum sea-level pressure (SLP) overlays the area of deep convection in the SAS during convective years (Fig. 9d, e).

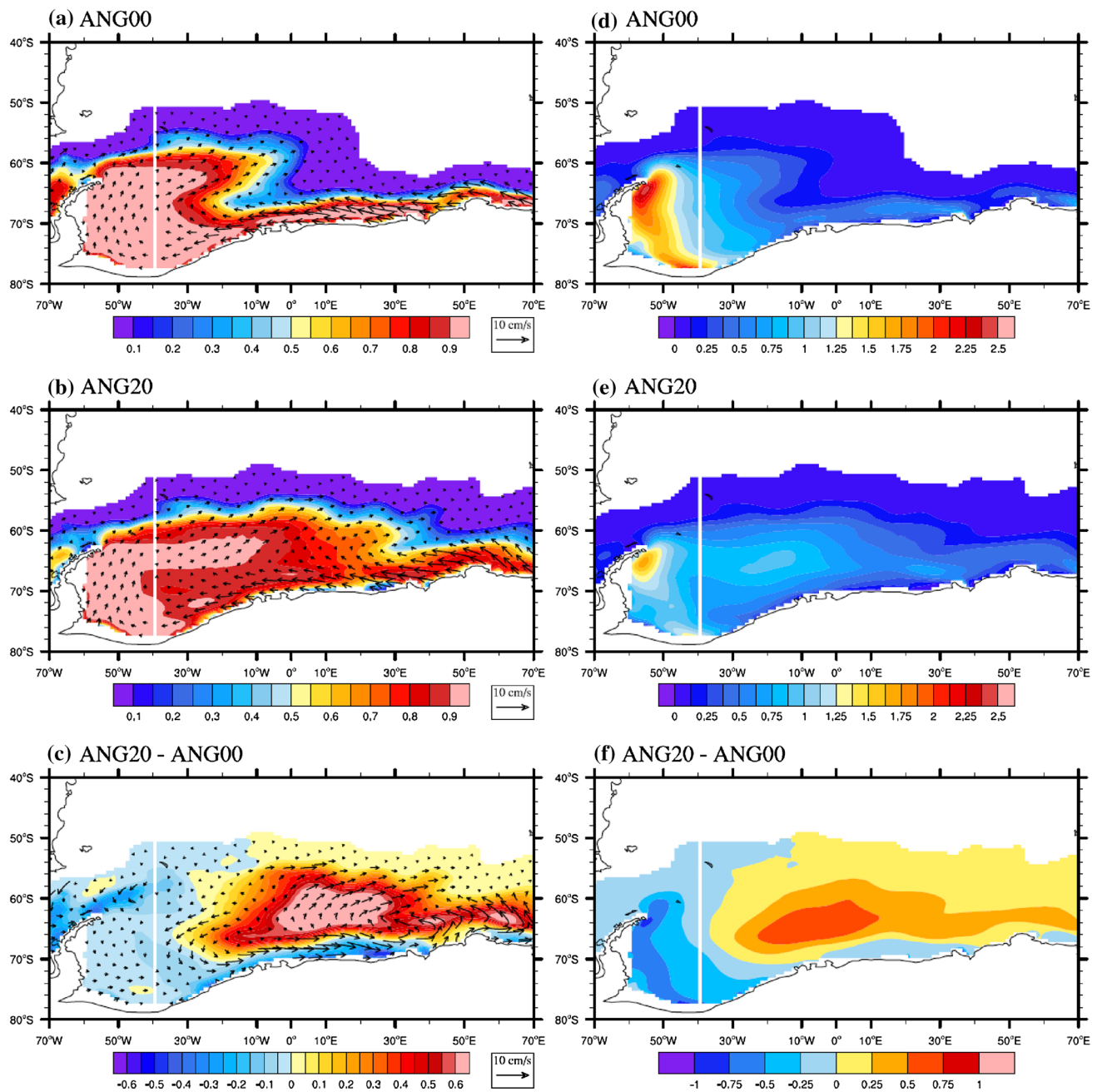


**Fig. 8** JJA-mean sea-ice drift (vector; cm/s) and sea-ice concentration (shading) (left panels) and sea-ice thickness (m; right panels) averaged over convective years in (a, d) ANG00 and (b, e) ANG20; and (c, f) difference between ANG00 and ANG20

ANG00 has stronger westerly in the open ocean of the SAS, whereas ANG20 has higher SLP there. The enhanced westerly forcing potentially induces more frequent occurrence of open-ocean deep convection in ANG00 (e.g., Cheon et al. 2014, 2015, 2018). The rising SLP of ANG20 with the cooling atmosphere weakens the cyclonic circulation (shown by vectors in Fig. 9f). The anticyclonic wind anomaly dampens, which slows down the cyclonic gyre in the SAS (Fig. 5c), and weakens the open-ocean deep convection in ANG20.

## 6 Understanding the response of Southern Ocean deep convection to sea ice–ocean stress

### 6.1 Continental shelf slope convection

Continental shelf slope convection is known to be closely linked to the formation of dense water that reaches the ocean bottom by descending along continental slope (Killworth

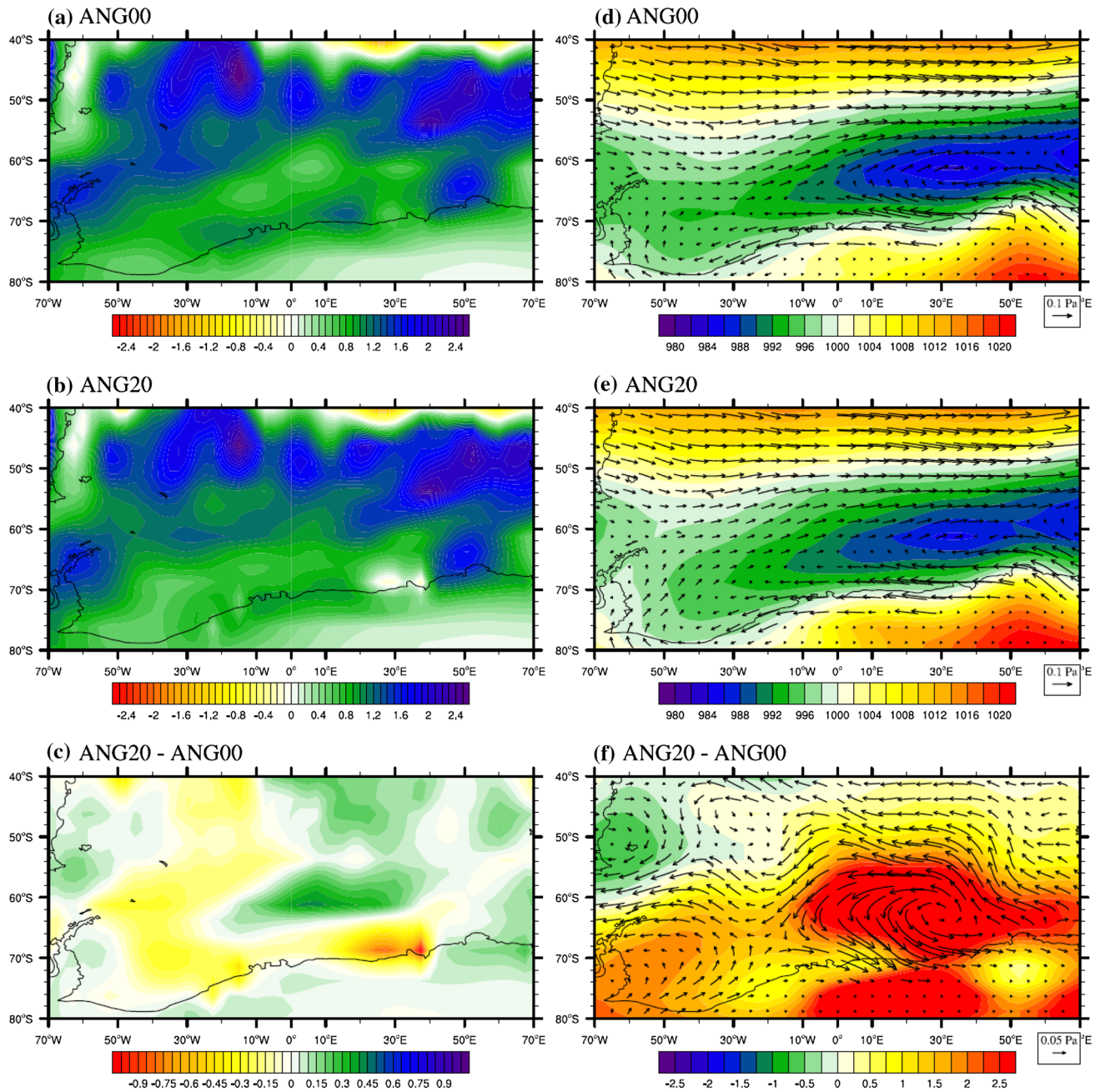


**Fig. 9** Same as Fig. 8, except for (left panels) freshwater flux ( $P-E$ ; mm/day) and (right panels) surface wind stress (vector; Pa) and sea-level pressure (shading; hPa)

1983). In addition, the formation of dense water is associated with the increased salinity induced by the brine rejection and reduced freshwater flux. Although coarse horizontal resolution is used in our model, the offshore katabatic winds are simulated in the southwestern Weddell Sea (Fig. 9d, e). Moreover, the enhanced cyclonic wind forcing is found in the southwestern Weddell Sea in ANG20, compared to ANG00 (Fig. 9f), indicating the coastal polynyas are prone to occur in ANG20 (Morales Maqueda et al. 2004; Williams

et al. 2007; Cappelletti et al. 2010; Rusciano et al. 2013). Note that the coarse ocean-model resolution used in this study is not sufficient to represent the continental slope topography. Thus, the physical processes discussed here are for a heuristic view. Figure 10 shows the JJA-mean net salt flux, which consists of the two parts attributed to the melting and freezing of sea ice, released from the sea ice to the ocean during convective years. Compared to ANG00, a large area with a salt flux from sea ice to ocean is found in the

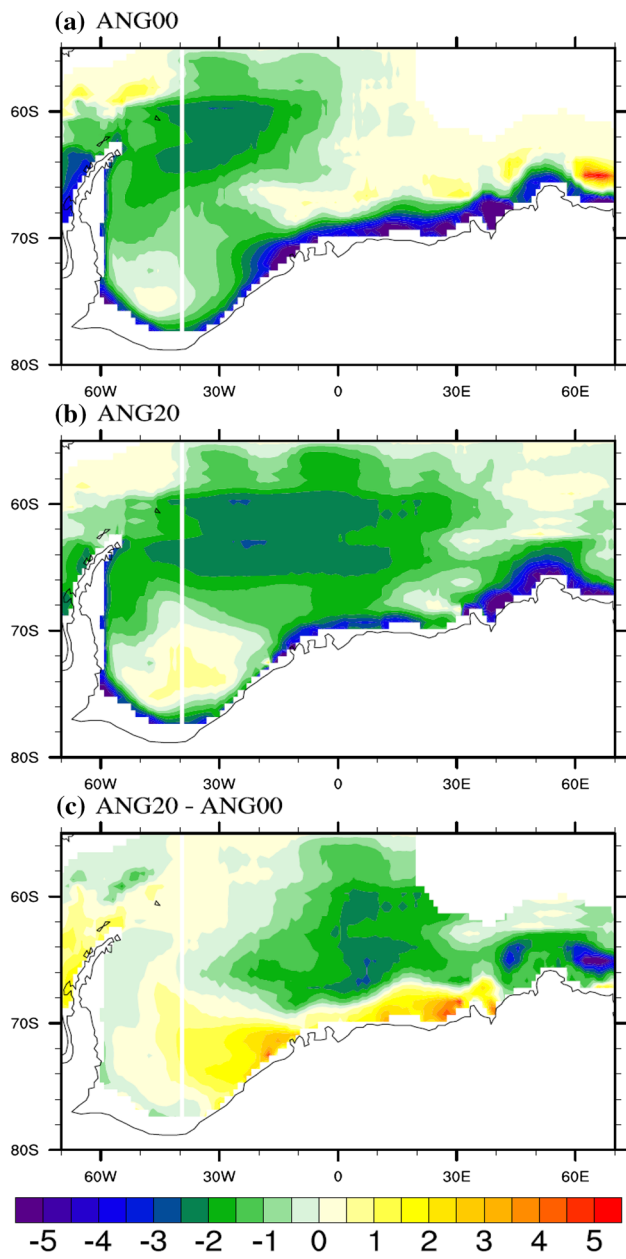


**Fig. 10** Same as Fig. 8, except for the net salt flux ( $10^{-7} \text{ kg/m}^2/\text{s}$ ) from sea ice to ocean

southwestern Weddell Sea in ANG20 (Fig. 10a, b), which is visible in the difference plot (Fig. 10c). Moreover, more precipitation and stronger evaporation are found in ANG20 compared to ANG00, and the increase in evaporation is larger than that in precipitation (figure not shown). Thus, the negative freshwater flux is found in the southwestern Weddell Sea (Fig. 9c). The combined effects of salt and freshwater flux contribute to the salinity increase of salinity in the southwestern Weddell Sea in ANG20 compared to ANG00. Although the difference of salt flux is positive in the coastal region in the southern SAS (Fig. 10c), the means state is

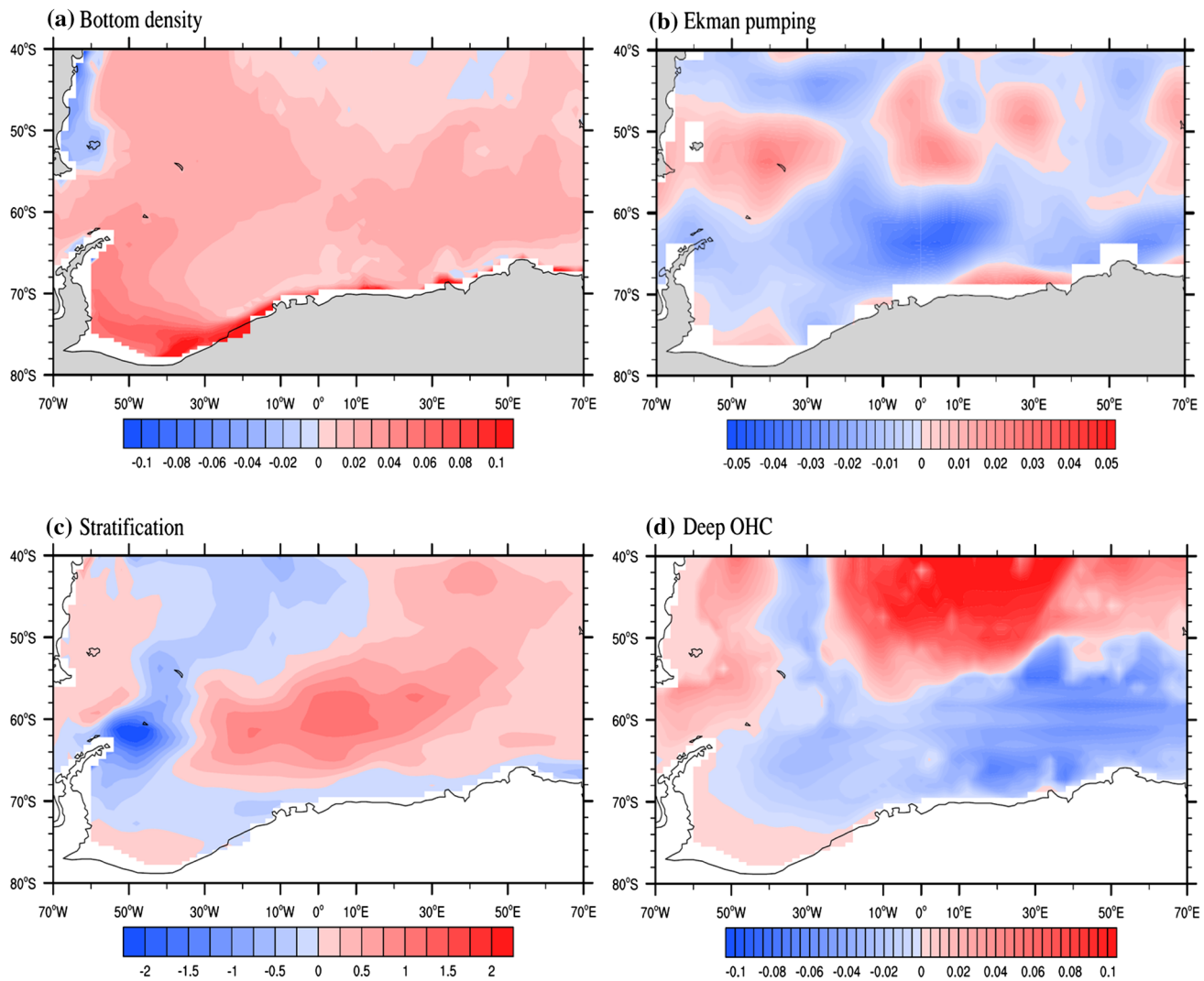
negative in ANG00 and ANG20 (Fig. 10a, b), indicating the increased salinity along the coastal region found in ANG20 (Fig. 4f) is dominated by the freshwater flux (Fig. 9c).

Figure 11a shows the difference in bottom potential density between ANG00 and ANG20 during convective years. We can see that the bottom water with a larger potential density is found in ANG20 compared to ANG00. Furthermore, the largest difference of potential density is found along the coastal region, implying that the denser water masses are formed along the coastal region in ANG20, where they descend along the continental slope. Thus, the enhanced continental shelf slope convection in ANG20 is due to the formation of denser water descending along the continental slope, which is attributed to the enhanced salt flux from the sea ice to the ocean and the freshwater flux from the atmosphere to the ocean. Figure 11b shows stronger Ekman pumping along the coastal region in the SAS in ANG20, implying that more warm deep water is upwelled to the surface to melt the sea ice. Moreover, descending denser surface water and enhanced Ekman pumping lead to a weakened stratification along the coastal region in the SAS in ANG20 compared to ANG00 (Fig. 11c).

## 6.2 Open-ocean deep convection

The open-ocean deep convection located in the eastern SAS is largely reduced in ANG20 compared to ANG00 (Fig. 4c, d). Thus, a question arises, whether the incorporation of non-zero turning angle is unfavorable for the occurrence of open-ocean deep convection? As discussed in Sect. 4, the weakened westerlies accompanying weakened cyclonic gyre in the SAS, enhanced freshwater flux, and increased sea-ice concentration in ANG20 play central roles in the reduction of open-ocean deep convection (Gordon et al. 2007; Galbraith et al. 2011; Cheon et al. 2014, 2018; de Lavergne et al. 2014). In addition, the variabilities of stability (Gordon and Huber 1990) and deep-ocean heat content (Cheon et al. 2015) exert influences on the variation of open-ocean deep convection. The difference of JJA-mean deep-ocean heat content between ANG00 and ANG20 is shown in Fig. 11d. Compared to the ANG00, a smaller ocean heat content is found in the open ocean in ANG20, suggesting that less oceanic heat flux is upwelled from the deep ocean to the surface to melt sea ice. Weakened Ekman pumping and enhanced stratification of sea water are found in the open SAS in ANG20 compared to ANG00 (Fig. 11b, c), which inhibits the overturning of water mass between the deep ocean and the surface layer, and limits the warm deep water to be upwelled to the surface layer.

Figure 12 shows time series of sea-ice concentration, maximum zonal-mean wind stress, freshwater flux, and deep-ocean heat content in terms of differences between ANG00 and ANG20. To estimate the maximum zonal-mean



**Fig. 11** Difference of JJA-mean **a** potential density at ocean bottom ( $\text{kg/m}^3$ ), **b** Ekman pumping ( $10^{-5} \text{ m/s}$ ), **c** stratification ( $10^{-5}/\text{s}$ ), and **d** deep-ocean heat content ( $10^{19} \text{ J}$ ) between ANG20 and ANG00. The

deep-ocean heat content is estimated below the depth of 1500 m. The stratification is calculated by using buoyancy frequency and is averaged value over the upper 2000 m

wind stress, the zonal mean of zonal wind stress is calculated over the longitudinal range  $60^\circ\text{W}$ – $60^\circ\text{E}$ ; then the maxima between  $80^\circ\text{S}$  and  $50^\circ\text{S}$  are derived. The other three time series plotted in Fig. 12 are the mean values, which are area-averaged over the open ocean ( $30^\circ\text{W}$ – $30^\circ\text{E}$ ,  $65^\circ$ – $55^\circ\text{S}$ ). As shown in Fig. 12a, the increased sea-ice concentration is generally associated with weakened zonal wind stress in ANG20 compared to ANG00, which confirms the conclusion that intensified westerlies potentially excite enhanced open-ocean deep convection (e.g., Cheon et al. 2018). An opposite relationship is found between sea-ice concentration and freshwater flux (Fig. 12b); that is, increased sea-ice concentration in ANG20 is generally associated with increased freshwater flux. Compared to ANG00, on the other hand, reduced deep-ocean heat content (Fig. 12c) and enhanced stability of sea water (Fig. 12d) are found in ANG20,

indicating that both contribute to the variability of sea-ice concentration, as well as the open-ocean deep convection in the SAS.

### 6.3 Discussion

The westerlies in the SO significantly are known to modulate open-ocean deep convection (Cheon et al. 2014, 2015, 2018). Moreover, our discussion in Sect. 6.2 indicates that weakened westerlies in ANG20 play a vital role in inhibiting the occurrence of open-ocean deep convection. In addition, enhanced northward sea-ice drift is found in the open ocean in ANG20 compared to ANG00 (Fig. 8c). In terms of time series of area-averaged difference between ANG20 and ANG00 over the open ocean, the correlation between JJA-mean sea-ice concentration and MAM-mean

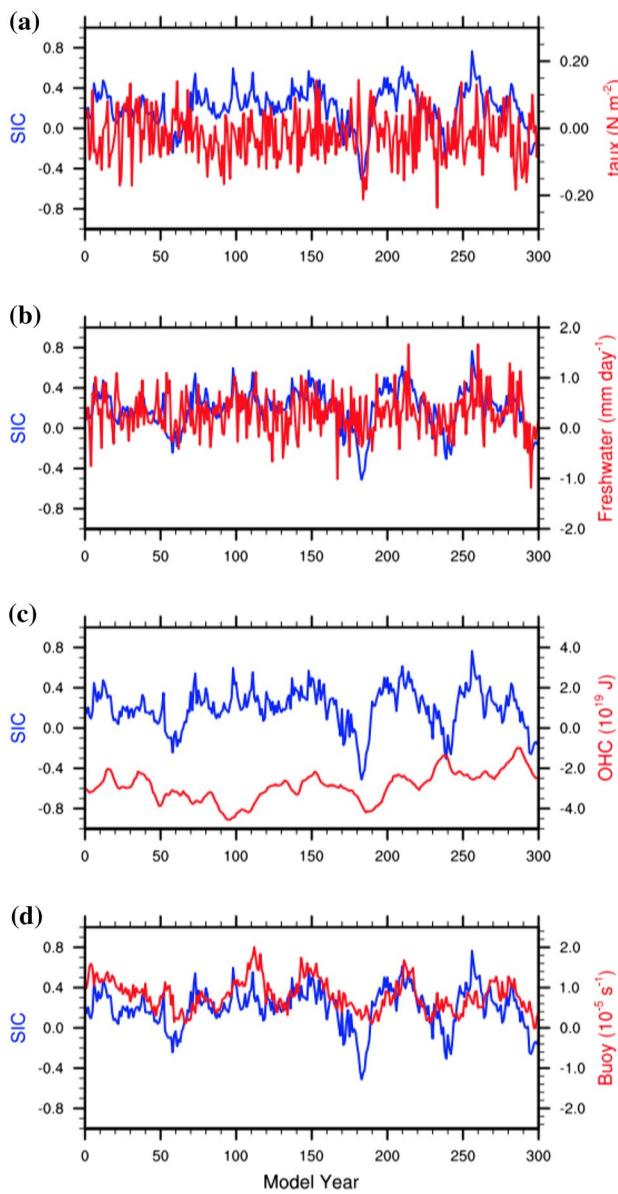


**Fig. 12** Time series of differences of sea-ice concentration and **a** maximum zonal-mean wind stress, **b** freshwater flux, **c** deep-ocean heat content, and **d** stratification between ANG20 and ANG00

(March–April–May-mean) maximal zonal-mean wind stress is 0.28, whilst the correlation between JJA-mean sea-ice concentration and JJA-mean maximal zonal-mean wind stress is 0.15, indicating that change in the maximal zonal-mean wind stress leads the change in sea-ice concentration. This is consistent with the conclusion of Cheon et al. (2018), that is, an increase of maximal zonal-mean wind precedes the occurrence of open-ocean deep convection. Is the enhanced northward sea-ice drift in ANG20 closely linked to the weakened westerlies? To verify this, experiment ANG00\_WND20 was conducted. In addition to clarify how ocean responds to the change in surface

wind stress, ANG00\_WND20 can help us clarify the following. (1) Whether the surface wind stress obtained from ANG20 alone can enhance the sea-ice divergence in the open ocean. (2) If it can, whether the enhanced sea-ice divergence can induce weakened open-ocean deep convection in the SAS.

Previous studies pointed out that the sea-ice divergence plays a central role in modulating open-ocean deep convection through northward transport of sea-ice freshwater (e.g., Saenko et al. 2002; Born et al. 2010; Sigman et al. 2010; Ferrari et al. 2014; Frölicher et al. 2015). Figure 13 depicts the JJA-mean sea-ice concentration, drift, and freshwater transport, which are averaged over the convective years, in ANG00 and ANG00\_WND20, and their differences. By comparing the sea-ice drift and concentration between ANG20 and ANG00\_WND20, we can see major differences in the western part and coastal region in the SAS (Figs. 8b, 13b), where larger sea-ice concentration exists. Thus, more sea ice is found in the western part and coastal region in the SAS in ANG00\_WND20 compared to ANG00 (Fig. 13c). Similar results are found in the open SAS between ANG20 and ANG00\_WND20. Moreover, compared to ANG00, ANG00\_WND20 has enhanced northward sea-ice freshwater transport in the SAS, which is associated with the intensified sea-ice divergence (Fig. 13d–f). Similar analyses conducted in Sect. 5 indicate that the intensified northward sea-ice freshwater transport in ANG00\_WND20 dilutes and cools the sea water in the open SAS compared to ANG00. On the other hand, similar results for the changes in SLP and freshwater flux are obtained. These results confirm that it is the change in the surface wind forcing that enhances the northward sea-ice freshwater transport in the SAS. As a result, the intensified northward sea-ice freshwater transport further modulates the atmosphere–sea ice–ocean interaction in the coupled climate system, including changes in the atmosphere, i.e., the SLP and freshwater flux (Fig. S3).

Changes in the open-ocean deep convection eventually occur as the consequence of a series of physical processes involving the atmosphere–sea ice–ocean interaction. Figure 14 shows the time series of the convective area (averaged in the domain of  $30^{\circ}\text{W}$ – $45^{\circ}\text{E}$ ,  $70^{\circ}$ – $55^{\circ}\text{S}$ ) in September. Compared to ANG00, ANG00\_WND20 displays distinguished multi-decadal variation of the open-ocean deep convection. According to the criterion defined in Sect. 2, the frequency of the open-ocean deep convection in ANG00 is about 1.0, indicating the convective event happens in each austral winter. However, the frequency of the open-ocean deep convection in ANG00\_WND20 is dramatically decreased, which is only 0.58. In addition, ANG00\_WND20 has a smaller convective area of  $4.3 \times 10^5 \text{ km}^2$ , compared to  $9.7 \times 10^5 \text{ km}^2$  in ANG00. Thus, weakened open-ocean deep convection in ANG00\_WND20 implies that the wind-driven sea-ice divergence potentially modulates and reduces

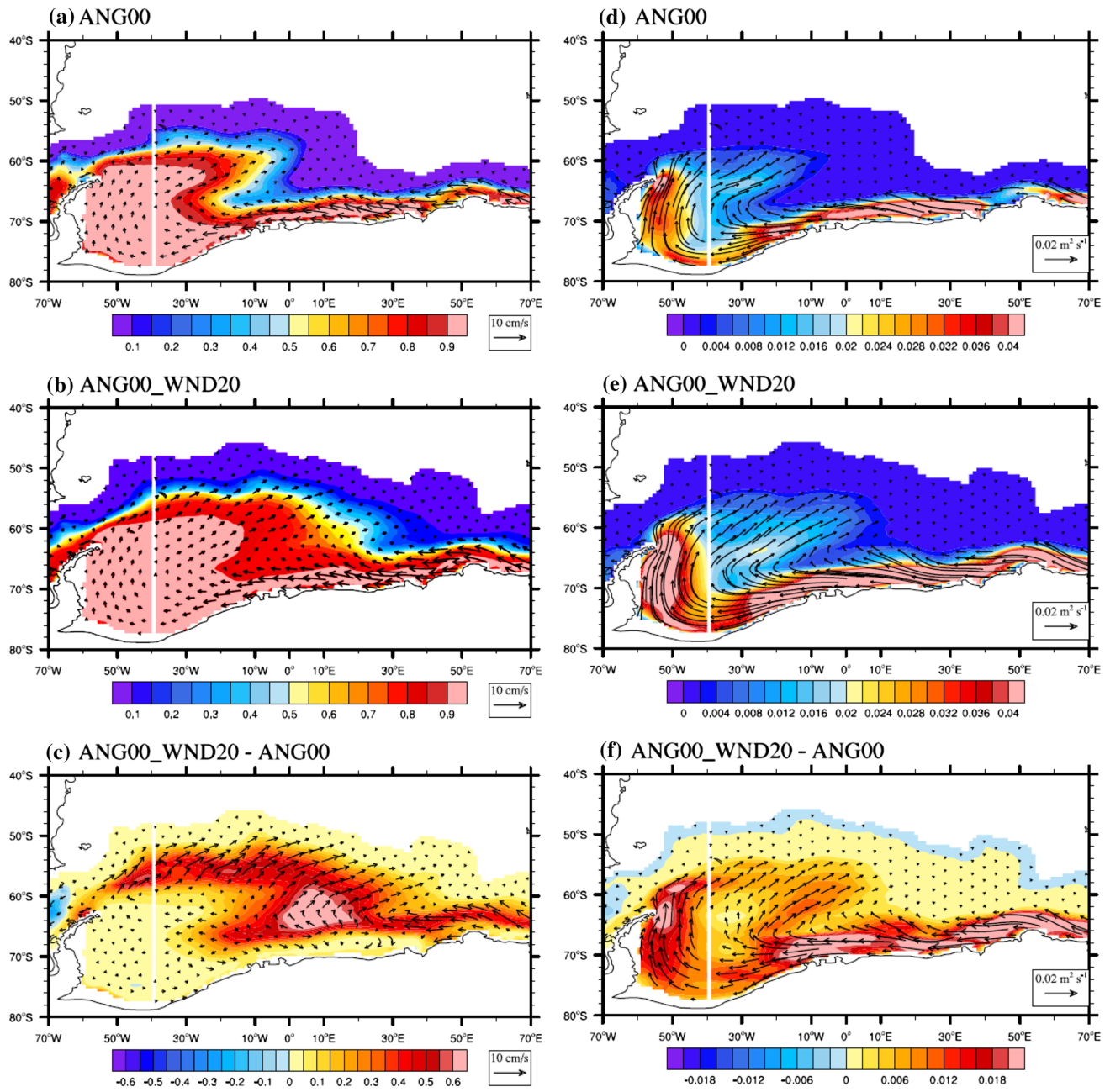


**Fig. 13** JJA-mean sea-ice drift (vector) and concentration (left panels) and sea-ice freshwater transport (vector) and its magnitude ( $\text{m}^2/\text{s}$ ; shading) (right panels) averaged over convective years of **a, d** ANG00 and **b, e** ANG00\_WND20; and **c, f** difference between ANG00\_WND20 and ANG00

open-ocean deep convection in the SAS through the atmosphere–sea ice–ocean interaction.

## 7 Concluding remarks

The turning angle between sea-ice relative velocity  $\mathbf{u}_i - \mathbf{u}_o$  and sea ice-ocean stress  $\boldsymbol{\tau}_{IO}$  can modulate the ice-ocean stress in a coupled climate model. Two sensitivity

experiments, referred to as ANG00 and ANG20 are conducted by setting the turning angle  $\beta$  to  $0^\circ$  and  $20^\circ$ , respectively. Changes in turning angle significantly modify the atmosphere–sea ice–ocean interaction in the SO, especially in the SAS, generating warmer and saltier coastal sea water and colder and fresher open-ocean sea water. The largest decreases in SST and SSS appear in the east of the SAS and the Ross Sea. In addition, using a non-zero turning angle can weaken the open-ocean deep convection and enhances

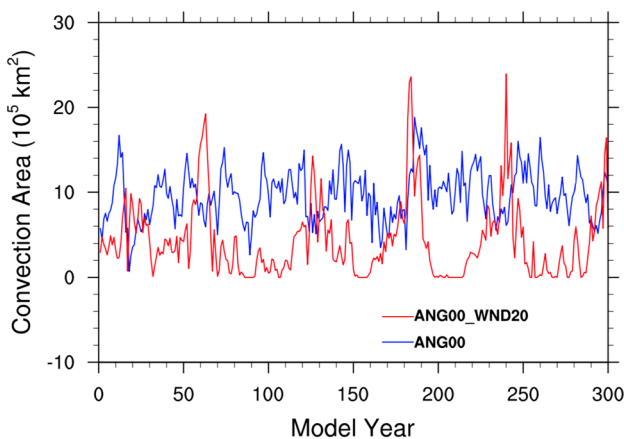


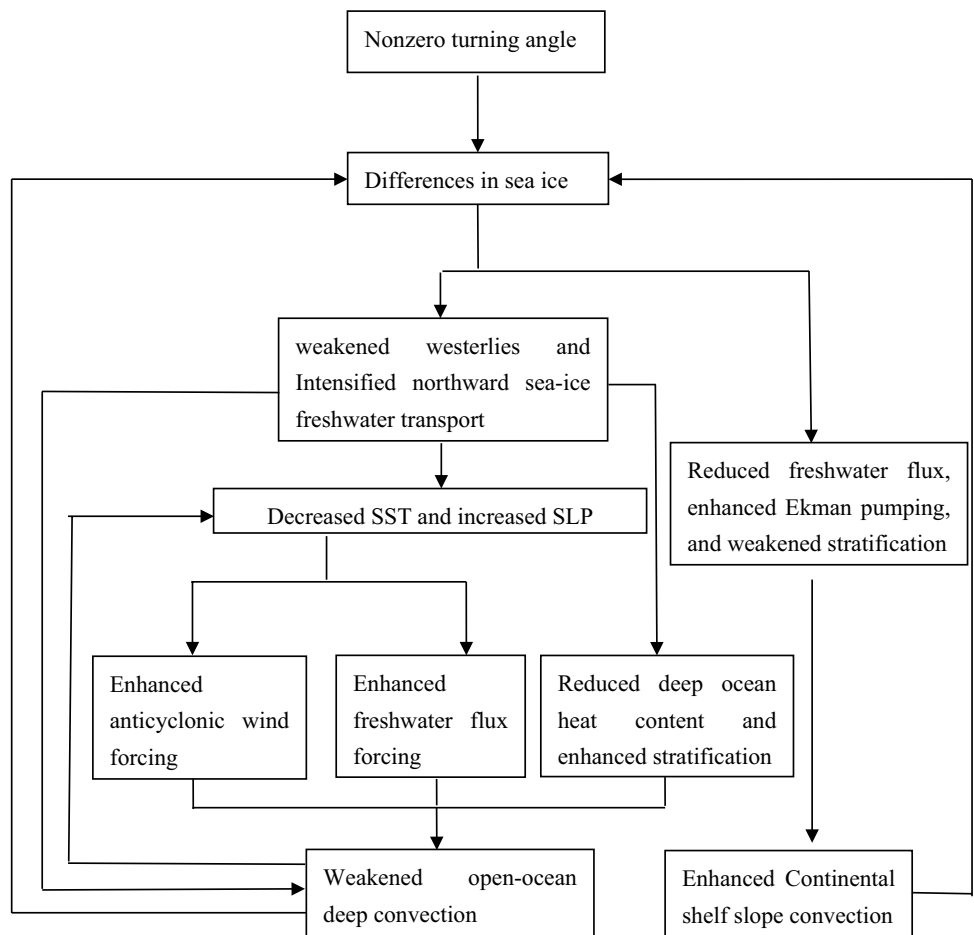
**Fig. 14** Time series of convective area ( $10^5 \text{ km}^2$ ) of ANG00 (blue curve) and ANG00\_WND20 (red curve) in September

the continental shelf slope convection in terms of strength and frequency.

The mechanism responsible for the changes in SO deep convection is explored and summarized in a schematic diagram (Fig. 15). A non-zero turning angle between the

relative velocity and sea ice–ocean stress, acts as a trigger, modifies atmosphere–sea ice–ocean interaction and leads to differences of sea ice in the SAS. In contrast, the usage of non-zero turning angle enhances the export of sea ice to the open SO, causing an increase of sea-ice concentration in the open ocean and a decrease near the coast (left panels in Fig. S4). Moreover, the northward sea-ice freshwater transport is intensified (right panels in Fig. S4), which tends to dilute and cool the sea water in the open SAS. Changes in sea-ice state, including sea-ice concentration and sea-ice albedo, lead to atmospheric changes. The increased sea-ice cover and albedo in the open SO weakens the surface wind stress and enhances the SLP (left panels in Fig. S5). In addition, the freshwater flux is intensified over the open SO, and is decreased over the SO coastal region including the southwestern corner of the Weddell Sea (right panels in Fig. S5). In response to the changes in surface wind stress, the cyclonic circulation is weakened and the SST is decreased in the SO (Fig. S6). Moreover, decreased SST further cools the surface air temperature and increases the SLP, and decreases the surface wind stress. Thus, the model with non-zero turning angle finally reaches a new climate state after all the feedback processes are adjusted.

**Fig. 15** Schematic diagram showing the atmosphere–sea ice–ocean interaction processes that control the response of deep convection to variation of sea ice–ocean stress



In the coastal region of the SO, the resulting enhanced salt flux from sea ice to the ocean reduced freshwater flux, enhanced Ekman pumping, and weakened stratification in the SAS coastal region, which enhance the formation of denser surface water, strengthen the continental shelf slope convection. On the other hand, weakened westerlies accompanying weakened cyclonic wind forcing lead to a reduced Ekman pumping, reduced deep-ocean heat content, and enhanced stratification in the open SAS. Additionally, increased sea-ice cover in the open SAS decreases SST and raises SLP, which further enhance the anticyclonic wind anomalies and freshwater flux forcing. The combined effect of ocean processes and atmospheric forcing contributes to the weakened open–ocean deep convection in the SAS. The sensitivity experiment ANG00\_WND20 confirms that the weakened westerlies accompanying weakened cyclonic wind field generated by the non-zero turning angle are capable of weakening the open–ocean deep convection in the SAS through enhancing the northward sea-ice freshwater transport. In turn, the weakened open–ocean deep convection, which cools the SST and increases the SLP in the open SAS, and enhanced continental shelf slope convection, which increases the SSS, lead to the increase of sea ice in the open SAS and reduction of sea ice in the SAS coastal region, establishing a positive feedback process.

The results in this study imply that changes in turning angle can regulate the occurrence and strength of the SO open–ocean deep convection (Fig. 4). The weakened open–ocean deep convection can potentially alleviate the SO warm bias in model (Fig. 5), a common problem in CMIP5 models (e.g., Wang et al. 2014; Schneider and Reusch 2016; Hyder et al. 2018). Moreover, the weakened open–ocean deep convection can induce changes in the Southern Annular Mode, as well as in the SO westerlies, which could weaken the SO upwelling (Anderson et al. 2009) and the formation of the Antarctic Bottom Water (AABW). In addition, changes in SO upwelling and the AABW formation are closely related to the variability of the AMOC (Marshall and Speer 2012), which impacts the global climate variability on decadal to centennial timescales (Park and Latif 2008; Galbraith et al. 2011; Martin et al. 2013). Thus, adequate parameterization of sea ice–ocean coupling, i.e., description of sea ice–ocean stress in CSMs, is important.

In this work, we simply selected two turning angles to discuss the influence of ice–ocean stress on the deep convection in the SO. However, the drag coefficient can also modulate the ice–ocean stress as shown by Eq. (2). Tsamados et al. (2014) argued that the drag coefficient between sea ice and ocean is variable. They decomposed the ice–ocean drag into skin and form drags, and the form drag includes the contribution of the keel and floe edge. On the other hand, McPhee (2012) suggested that both turning angle and drag coefficient vary with the speed of sea ice at

a given undersurface hydraulic roughness. This indicates that current settings of turning angle and drag coefficient of ice–ocean stress in NESM3.0 may be too simple, and improved parameterization needs to be considered in the future. These improvements will be implemented in the next generation of NESM. Further analyses will also be conducted to discuss the impact of improved ice–ocean stress on the variability of ocean circulation, including the open–ocean deep convection and transport of the Antarctic Circumpolar Current.

**Acknowledgements** This study is supported by the grant 2018YFA0605904 from the National Major Research High Resolution Sea Ice Model Development Program of China. This study is also sponsored by the Basic Research Fund of CAMS (2018Z007) and the Startup Foundation for Introducing Talent of NUIST (No. 2018r064). This is the IPRC publication number 1435 and ESMC publication number 303.

## References

- Akitomo K (1999a) Open–ocean deep convection due to thermobaricity 1. Scaling argument. *J Geophys Res* 104:5225–5234
- Akitomo K (1999b) Open–ocean deep convection due to thermobaricity 2. Numerical experiments. *J Geophys Res* 104:5235–5249
- Anderson RF, Ali S, Bradtmiller LI, Nielsen SHH et al (2009) Wind-driven upwelling in the Southern Ocean and the Deglacial Rise in atmospheric CO<sub>2</sub>. *Science* 323:1443–1448
- Balmaseda MA, Mogensen K, Weaver AT (2013) Evaluation of the ECMWF ocean reanalysis system ORAS4. *QJR Meteorol Soc* 139:1132–1161
- Behrens E, Rickard G, Morgenstern O, Martin T, Osprey A, Joshi M (2016) Southern Ocean deep convection in global climate models: a driver for variability of subpolar gyres and Drake Passage transport on decadal timescales. *J Geophys Res Oceans* 121:3905–3925
- Born A, Nisancioglu KH, Braconnot P (2010) Sea ice induced changes in ocean circulation during the Eemian. *Climate Dyn* 35:1361–1371
- Cao J, Wang B, Yang YM, Ma LB et al (2018) The NUIST Earth System Model (NESM) version 3: description and preliminary evaluation. *Geosci Model Dev* 11:2975–2993
- Cappelletti A, Picco P, Peluso T (2010) Upper ocean layer dynamics and response to atmospheric forcing in the Terra Nova Bay polynya, Antarctica. *Antarct Sci* 22(3):319–329
- Cheon WG, Park YG, Toggweiler JR, Lee SK (2014) The relationship of Weddell Polynya and open–ocean deep convection to the Southern Hemisphere westerlies. *J Phys Oceanogr* 44:694–713
- Cheon WG, Lee S-K, Gordon AL et al (2015) Replicating the 1970’s Weddell Polynya using a coupled ocean-sea ice model with reanalysis surface flux fields. *Geophys Res Lett* 42:5411–5418
- Cheon WG, Cho C-B, Gordon AL et al (2018) The role of oscillating Southern Hemisphere westerly winds: Southern Ocean coastal and open–ocean polynyas. *J Climate* 31:1053–1073
- Chu PC (2015) Ekman spiral in a horizontally inhomogeneous ocean with varying eddy viscosity. *Pure Appl Geophys* 172:2831–2857
- Danabasoglu G (2008) On multidecadal variability of the Atlantic Meridional overturning circulation in the Community Climate system model version 3. *J Climate* 21:5524–5544
- Defant A (1961) Physical oceanography, vol 1. Pergamon Press, Oxford

- de Lavergne C, Palter JB, Galbraith ED, Bernardello R, Marinov I (2014) Cessation of deep convection in the open Southern Ocean under anthropogenic climate change. *Nat Climate Change* 4:278–282
- Delworth T, Manabe S, Stouffer RJ (1993) Interdecadal variations of the thermohaline circulation in a coupled ocean-atmosphere model. *J Climate* 6:1993–2011
- Dong B, Sutton R (2001) The dominant mechanisms of variability in Atlantic Ocean heat transport in a coupled ocean-atmospheric GCM. *Geophys Res Lett* 28:2445–2448
- Fahrbach E, Rohardt G, Scheele N, Schröder M, Strass V, Wisotzki A (1995) Formation and discharge of deep and bottom water in the northwestern Weddell Sea. *J Mar Res* 53:515–538
- Ferrari R et al (2014) Antarctic sea ice control on ocean circulation in present and glacial climates. *Proc Natl Acad Sci USA* 111:8753–8758
- Frankignoul C, Deshayes J, Curry R (2009) The role of salinity in the decadal variability of the North Atlantic meridional overturning circulation. *Climate Dyn* 33:777–793
- Frölicher TL et al (2015) Dominance of the Southern Ocean in anthropogenic carbon and heat uptake in CMIP5 models. *J Climate* 28:862–886
- Galbraith ED et al (2011) Climate variability and radiocarbon in the CM2MC Earth System Model. *J Climate* 24:4230–4254
- Ge X, Wang W, Kumar A, Zhang Y (2017) Importance of the vertical resolution in simulating SST diurnal and intraseasonal variability in an oceanic general circulation model. *J Clim* 30(11):3963–3978
- Gordon AL (1978) Deep Antarctic convection west of Maud Rise. *J Phys Oceanogr* 8:600–612
- Gordon AL (1982) Weddell deep water variability. *J Mar Res* 40:199–217
- Gordon AL, Comiso JC (1987) Polynyas in the southern ocean. *Sci Am* 256:90–97
- Gordon AL, Huber BA (1990) Southern Ocean winter mixed layer. *J Geophys Res* 95:11655–11672
- Gordon AL, Visbeck M, Comiso JC (2007) A possible link between the Weddell polynya and the Southern Annular Mode. *J Climate* 20:2558–2571
- Haumann FA, Gruber N, Münnich M, Frenger I, Kern S (2016) Sea-ice transport driving Southern Ocean salinity and its recent trends. *Nature* 537:89–92
- Heuzé C, Heywood KJ, Stevens DP, Ridley JK (2013) Southern Ocean bottom water characteristics in CMIP5 models. *Geophys Res Lett* 40:1409–1414
- Hirabara M, Tsujino H, Nakano H, Yamanaka G (2012) Formation mechanism of the Weddell Sea Polynya and the impact on the global abyssal ocean. *J Oceanogr* 68:771–796
- Holland DM (2001) Explaining the Weddell Polynya—a large ocean eddy shed at Maud Rise. *Science* 292:1697–1700
- Hunke EC (2010) Thickness sensitivities in the CICE sea ice model. *Ocean Model* 34:137–149
- Hunke EC, Lipscomb WH (2010) CICE: the Los Alamos Sea Ice Model documentation and software user's manual version 4.1. LA-CC-06-012, p 76
- Hunkins K (1966) Ekman drift currents in the Arctic Ocean. *Deep Sea Res* 13:607–620
- Hurrell JW, Holland MM, Gent PR et al (2013) The community earth system model: a framework for collaborative research. *Bull Am Meteorol Soc* 9:1339–1360
- Hyder P, Edwards JM et al (2018) Critical Southern Ocean climate model biases traced to atmospheric model cloud errors. *Nat Commun* 9:3625. <https://doi.org/10.1038/s41467-018-056634-2>
- Jackson L, Vellinga M (2012) Multidecadal to centennial variability of the AMOC: HadCM3 and a perturbed physics ensemble. *J Climate* 26:2390–2407
- Killworth PD (1983) Deep convection in the world ocean. *Rev Geophys Space Phys* 21:1–26
- Madec G (2012) NEMO ocean engine. ISSN No 1288-1619, p 366
- Marshall J, Schott F (1999) Open-ocean deep convection: Observations, theory, and models. *Rev Geophys* 37:1–64
- Marshall J, Speer K (2012) Closure of the meridional overturning circulation through Southern Ocean upwelling. *Nat Geosci* 5:171–180
- Martin T, Park WS, Latif M (2013) Multi-centennial variability controlled by Southern Ocean convection in the Kiel Climate Model. *Climate Dyn* 40:2005–2022
- Martinson DG (1991) Deep convection and deep water formation in the oceans. In: Chu PC, Gascard JC (eds) Elsevier oceanography series, pp 37–52
- Martinson DG, Killworth PD, Gordon AL (1981) A convective model for the Weddell Polynya. *J Phys Oceanogr* 11:466–488
- McPhee MG (1980) An analysis of pack ice drift in summer. In: Pritchard R (ed) Sea ice processes and models. University of Washington Press, Seattle, pp 62–75
- McPhee MG (2012) Advances in understanding ice-ocean stress during and since AIDJEX. *Cold Region Sci Technol* 76–77:24–36
- Morales Maqueda MA, Willmott AJ, Biggs NRT (2004) Polynya dynamics: a review of observations and modeling. *Rev Geophys*. <https://doi.org/10.1029/2002RG000116>
- Morgenstern O, Zeng G, Dean SM, Hoshi M, Abraham NL, Osprey A (2014) Direct and ozone-mediated forcing in the Southern annual mode by greenhouse gas. *Geophys Res Lett* 41:9050–9057
- Msadek R, Frankignoul C (2009) Atlantic multidecadal oceanic variability and its influence on the atmosphere in a climate model. *Climate Dyn* 33:45–62
- Ohshima KI, Nakanowatari T, Riser S, Volkov Y, Wakatsuchi M (2014) Freshening and dense shelf water reduction in the Okhotsk Sea linked with sea ice decline. *Prog Oceanogr* 126:71–79
- Orsi AH, Johnson GC, Bullister JL (1999) Circulation, mixing, and production of Antarctic Bottom Water. *Prog Oceanogr* 43:55–109
- Park W, Latif M (2008) Multidecadal and multicentennial variability of the meridional overturning circulation. *Geophys Res Lett* 35:L22703. <https://doi.org/10.1029/2008GL035779>
- Park W, Keenlyside N, Latif M et al (2009) Tropical pacific climate and its response to global warming in the Kiel Climate Model. *J Climate* 22:71–92
- Raddatz TJ, Reick CH, Kattge J et al (2007) Will the tropical land biosphere dominate the climate-carbon cycle feedback during the twenty-first century? *Climate Dyn* 29:565–574
- Reintges A, Martin T, Latif M, Park W (2017) Physical controls of Southern Ocean deep-convection variability in CMIP5 models and the Kiel Climate Model. *Geophys Res Lett* 44:6951–6958
- Roberts CD, Garry FK, Jackson LC (2013) A multimodel study of sea surface temperature and subsurface density fingerprints of the Atlantic Meridional Overturning Circulation. *J Climate* 26:9155–9174
- Robertson R, Visbeck M, Gordon AL, Fahrbach E (2002) Longterm temperature trends in the deep waters of the Weddell Sea. *Deep Sea Res II* 49:4791–4806
- Rusciano E, Budillon G, Fusco G, Spezie G (2013) Evidence of atmosphere-sea ice-ocean coupling in the Terra Nova Bay polynya (Ross Sea—Antarctica). *Cont Shelf Res* 61–62:112–124
- Saenko OA, Schmittner A, Weaver AJ (2002) On the role of wind-driven sea ice motion on ocean ventilation. *J Phys Oceanogr* 32:3376–3395
- Schneider DP, Reusch DB (2016) Antarctic and southern ocean surface temperatures in CMIP5 models in the context of the surface energy budget. *J Climate* 29:1689–1716
- Sigman DM, Hain MP, Haug GH (2010) The polar ocean and glacial cycles in atmospheric CO<sub>2</sub> concentration. *Nature* 466:47–55

- Smith S, Muench RD, Pease CH (1990) Polynyas and leads: an overview of physical processes and environment. *J Geophys Res* 95:9461–9479
- Stevens B et al (2013) The atmospheric component of the MPI-M Earth System Model: ECHAM6. *J Adv Model Earth Syst* 5:146–172
- Tsamados M, Feltham DL, Schroeder D, Flocco D (2014) Impact of variable atmospheric and oceanic form drag on simulations of Arctic sea ice. *J Phys Oceanogr* 44:1329–1353
- Uotila P, O'Farrell S, Marsland SJ, Bi D (2012) A sea-ice sensitivity study with a global ocean-ice model. *Ocean Model* 51:1–18
- Valcke S, Coquart L (2015) OASIS-MCT user guide: OASIS-MCT 3.0. CERFACS TR/CMGC/15/38, p 58
- Wang CZ, Zhang LP, Lee S-K, Wu LX, Mechoso CR (2014) A global perspective on CMIP5 climate model biases. *Nat Climate Change* 4:201–205
- Wang ZM, Wu Y, Lin X, Liu CY, Xie ZL (2017) Impacts of open-ocean deep convection in the Weddell Sea on coastal and bottom water temperature. *Climate Dyn* 48:2967–2981
- Williams WJ, Carmarck EC, and Ingram RG (2007) Physical oceanography of polynyas. In: Smith W and Barber D (eds) Chap 2: Polynyas: windows to the world. Elsevier oceanography series, vol 74. Elsevier, pp 55–85
- Zika JD, Sommer JL, Dufour CO, Naveira-Garabato A, Blaker A (2013) Acceleration of the Antarctic circumpolar current by wind stress along the coast of Antarctica. *J Phys Oceanogr* 43:2772–2784

**Publisher's Note** Springer Nature remains neutral with regard to jurisdictional claims in published maps and institutional affiliations.

## Affiliations

Libin Ma<sup>1,2</sup> · Bin Wang<sup>3</sup> · Jian Cao<sup>2</sup>

<sup>1</sup> State Key Laboratory of Severe Weather, Chinese Academy of Meteorological Sciences, Beijing 100081, China

<sup>2</sup> Key Laboratory of Meteorological Disaster of Ministry of Education (KLME)/Joint International Research Laboratory of Climate and Environment Change (ILCEC)/Collaborative Innovation Center On Forecast and Evaluation of Meteorological Disasters (CIC-FEMD), Nanjing University of Information Science and Technology,

Ningliu Road 219, Meteorology Bldg, Nanjing 210044, Jiangsu, China

<sup>3</sup> Department of Atmospheric Sciences and International Pacific Research Center, School of Ocean and Earth Science and Technology, University of Hawaii at Manoa, 1860 East-West Road, POST Bldg. 401, Honolulu, HI 96822, USA